Reflection of underwater sound from surface waves

Chris T. Tindle
Physics Department, University of Auckland, Bag 92019, Auckland 1142, New Zealand

Grant B. Deane
Marine Physical Laboratory, Scripps Institution of Oceanography, UCSD, La Jolla, California 92093-0238

James C. Preisig
Woods Hole Oceanographic Institution, Woods Hole, Massachusetts 02543

(Received 26 February 2008; revised 28 October 2008; accepted 30 October 2008)

A tank experiment has been conducted to measure reflection of underwater sound from surface waves. Reflection from a wave crest leads to focusing and caustics and results in rapid variation in the received waveform as the surface wave moves. Theoretical results from wavefront modeling show that interference of three surface reflected eigenrays for each wave crest produces complicated interference waveforms. There is good agreement between theory and experiment even on the shadow side of caustics where there are two surface reflected arrivals but only one eigenray.
 [DOI: 10.1121/1.3035828]

PACS number(s): 43.30.Cq, 43.30.Dr, 43.30.Gv [JAC] Pages: 66–72

I. INTRODUCTION

The use of sound for underwater communications is made complicated by reflections from the ocean surface.[1] The crests of ocean surface waves act as curved reflectors for underwater sound, which can give focusing and multiple arrivals due to the reflection from different parts of a single crest. The purpose of this paper is to investigate this phenomenon using a time-domain wave front propagation model[2,3] and some scale-model tank experiments.

It is well known that a ray trace for underwater sound propagation in deep water with a sound speed minimum as a function of depth leads to the formation of foci and caustics.[4] The various types of caustics and the consequences for pulse propagation as a result of vertical structure in the sound speed profile are discussed in detail by Brown.[5] There is an extensive literature treating wave scattering from rough surfaces in the electromagnetic and acoustical literature (see Refs. 6 and 7 for reviews). The wavefront model used here was developed to treat reflection of broadband pulses from a deterministic, time-varying surface, and thus differs from stochastic treatments of scattering from random, rough surfaces. The work by Frederickson and Marston[8,9] and Williams *et al.*[10] is particularly relevant to the present study because of their analytical treatment and experimental studies of caustic formation for the case of tone bursts and transient signals reflected by curved surfaces. The experiments reported here are broadband and were specifically designed to test the fidelity of the wavefront model.[2,3]

The present study represents one end of a continuum of surface conditions with a smooth, correlated surface at one extreme and a rough, random surface at the other. The length scale dividing "smooth" from "rough" may be usefully assumed to be proportional to the length of a Fresnel zone and is thus related to the range of wavelengths associated with the acoustic pulse reflected from the surface in addition to the source-receiver geometry and prevailing surface conditions. In practice, sea surface conditions can present well-correlated swell from distant storms, a random, wind-driven wave spectrum, or a mixture of the two. Although it would be valuable to study the surface conditions under which the deterministic modeling approach adopted here fails, this study is restricted to monochromatic, smooth surface waves. When scaled to ocean waves of 10 s period, the experiment reported here is equivalent to transmission at 890 Hz over a distance of 275 m beneath smooth swell with peak to trough heights from 1.6 m up to 10.4 m

A tank experiment was conducted to undertake a detailed reconciliation between the wavefront model described in Refs. 2 and 3 and scale-model propagation measurements. The surface waves in the flume were controllable, uniform, and reproducible. The experiment used very short, high frequency acoustic pulses or "pings" and a short range so that surface reflections arrived before any reflections from the walls or bottom of the tank. It was necessary to allow reverberation to decay away between pings but a repetition rate of 180 pings/s was achieved. The results were recorded and show how the pulses reflected from the surface change in amplitude, phase, and arrival time as the wave progresses. The experimental results have been modeled to very good accuracy with the wavefront model, and this gives confidence that the reflection process beneath smooth surface waves is well understood.

II. THE EXPERIMENT

The experimental arrangement is shown schematically in Fig. 1. The experiment was conducted in a wave tank at Scripps Institution of Oceanography. The tank is 0.6 m wide and 30 m long. The water depth is a nominal 0.6 m. Waves are generated with a computer-controlled paddle at one end of the tank. For the present results, the surface wave frequency was 1.5 Hz with a wavelength of 0.693 m. The

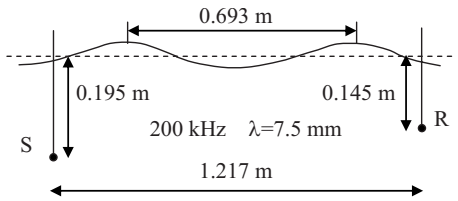

FIG. 1. Experimental arrangement. One cycle pulses at a nominal frequency of 200 kHz were transmitted from source S to receiver R under surface waves moving from left to right.

waves were uniform and repeatable from day to day. The wave height was constant for each run and varied up to a peak to trough height of 46 mm.

The acoustic source S and receiver R were ITC1089D SN transducers. Each transducer is a cylinder about 70 mm long and 10 mm diameter with the active element centered 5 mm from one end. The hydrophones were deployed horizontally, perpendicular to the direction of the waves and were omnidirectional for propagation along the tank. The depths of the nominal centers of the source and receiver transducers were determined by analyzing direct and surface reflected arrivals taken with a flat surface and were found to be 195 and 145 mm, respectively. The horizontal range was 1.217 m. The tank was filled with fresh water with a measured sound speed of 1469 m/s.

The instantaneous wave height near the source was measured to millimeter accuracy with a wave gauge composed of vertical parallel wires in a Wheatstone bridge arrangement. The surface wave speed, which was calculated using the known wave frequency, the measured mean water depth, and the full surface wave dispersion equation, was then used to find the instantaneous surface height as a function of horizontal displacement from the wave gauge. The data to be reported were identified as runs 101–106 and had peak to trough wave heights of 7, 16, 24, 31, 39, and 46 mm, respectively. Movies of experimental waveforms and modeling results for these runs can be viewed on EPAPS.[11]

Pulse transmission and data digitization were synchronized to the surface wave generator. A short pulse was transmitted at 180 pulses/s which gave 120 pulses per surface wave period. The waveform used to excite the source transducer was designed to compensate for the frequency-dependent amplitude and phase response of the ITC1089D ceramic element. The resulting pressure pulse in the water was nominally one cycle at 200 kHz (see the first arrival in Fig. 6). Although it would be possible to include a detailed electromechanical model of the transducers and their associated electronics in the propagation model, we have avoided this complication by using the observed direct arrival pulse at the receiver, averaged over 120 transmissions and scaled to account for geometric spreading, as the source pulse. This averaged pulse was then used directly as the source pulse in the wavefront calculations to model the acoustic field incident on the surface.

Data from the receiver were digitized at 1 538 461.54 samples/s for 6 153 846 samples or about 4 s, providing data for six complete surface waves. The received waveform for each pulse transmission was determined by averaging synchronized pulses over four complete waves, which served to reduce noise from electronic and acoustical sources and reduce any slight variability in reflection between successive wave crests. Initially wave profiles were measured simultaneously with the pulse transmissions. However, the waves were found to be highly repeatable from day to day so that later runs could use wave height data taken from earlier runs.

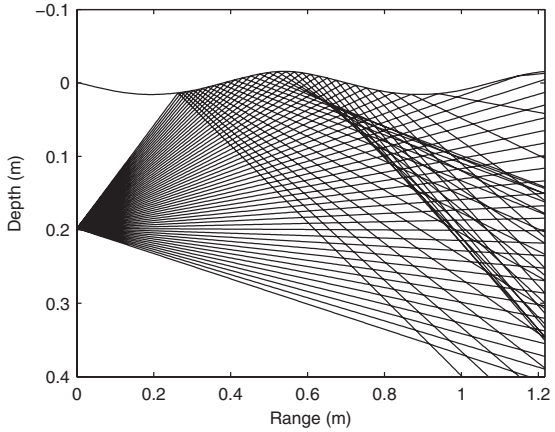

FIG. 2. Ray trace for run 104, ping 36.

III. WAVEFRONT MODELING

When the experimental results are presented, the waveforms will be compared with theoretical waveforms calculated using the wavefront modeling method described in Refs. 2 and 3. The calculations are based on the assumption that the surface can be considered stationary during a single pulse transmission. There are Doppler shifts associated with the movement of the surface, which the current model does not account for but which can be seen in data taken from transmission experiments in the surf zone. Doppler shifts could be included but are not necessary for the present analysis.

Wavefront modeling begins with a ray trace, a representative example of which is shown in Fig. 2. The ray trace is for ping 36 in run 104. The waves had a peak to trough wave height of 31 mm and the waves are traveling from left to right.

In Fig. 2, the wave crest is just before the midrange position, and the rays are focused by the crest to converge about 50 mm below the surface at a range of about 0.7 m. After passing through the focus the rays diverge to form a fan with well-defined boundaries, which are caustics for the ray field. The eigenray paths are shown in Fig. 3 for the same wave position shown in Fig. 2. There are three distinct surface reflected rays reaching the receiver.

As the surface wave moves, the number of eigenrays and the angles of the eigenrays change. When the wave crest is near the middle of the range there are typically three eigenrays, as shown in Fig. 3. When there is a trough near the middle of the range there is only one eigenray. As the wave progresses the position of the focus and the caustics in Fig. 2 changes, and the caustics sweep upward through the receiver position. When the receiver is between the caustics

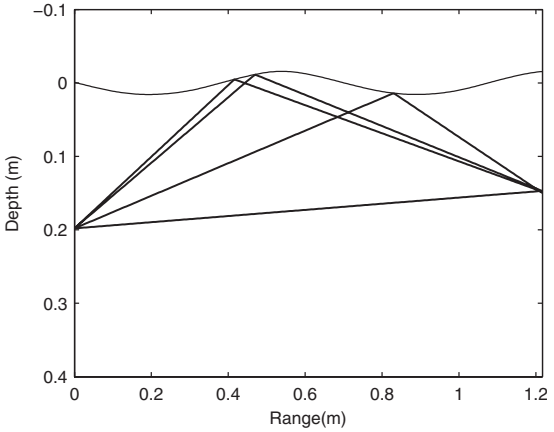

FIG. 3. Eigenrays for the ray trace of Fig. 2.

there are three eigenrays but there is only one eigenray when it is outside. The eigenrays appear or disappear in pairs as a caustic passes the receiver.

The ray trace is used in the wavefront modeling method to determine the depth z^* of a ray at the range of the receiver as a function of its angle θ at the source. A graph of z^* as a function of θ for the same situation shown in Fig. 2 is shown in Fig. 4.

The angles in Fig. 4 are negative because we have adopted the convention of distance measured positive downward from the mean surface. As the ray angle increases the depth of the ray at the receiver range decreases to a minimum at about −25°. This minimum corresponds to the upper caustic in Fig. 2. Further increase in ray angle leads to a maximum depth at about −18° which corresponds to the lower caustic in Fig. 2. Further increase in ray angle shows that the ray meets the surface for a ray angle of about −10°. Further increase in ray angle from −10° to 0° gives an almost linear increase in depth as the ray passes the receiver range without hitting the surface.

The line at a depth of 0.145 m in Fig. 4 corresponds to the depth of the receiver. Intersections of the line and the curve occur when the depth of the ray at the receiver range corresponds to the receiver depth. The intersections determine the angles for the eigenrays of Fig. 3. The direct ray has

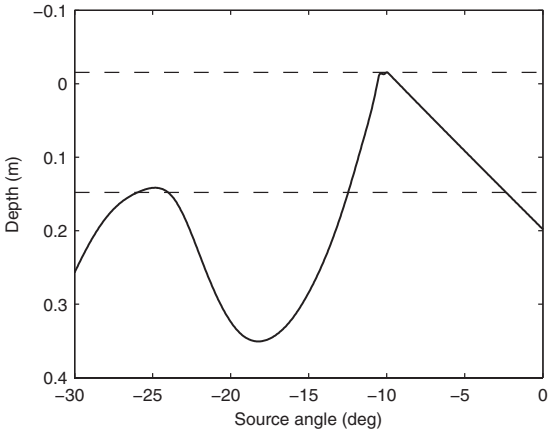

FIG. 4. Ray depth $z^*(\theta)$ at the receiver range as a function of launch angle θ. The upper dashed line is the ocean surface at the range of the receiver. The lower dashed line is the receiver depth.

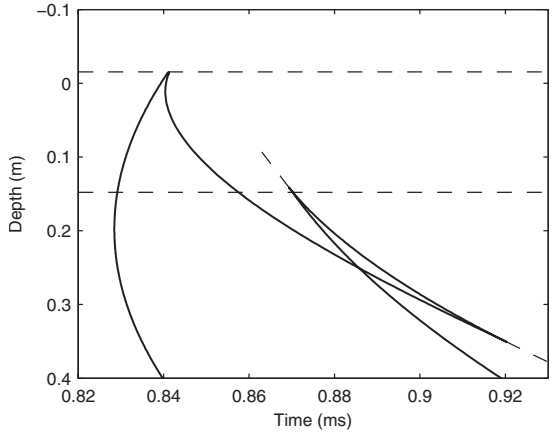

FIG. 5. Ray depth at the receiver range as a function of arrival time. The upper dashed line is the surface at the range of the receiver. The lower dashed line is the receiver depth.

a source angle of about −2° and the surface reflected rays have source angles of about −26°, −24°, and −12°.

The ray trace of the wavefront model is also used to find the ray travel time to the range of the receiver along each ray path. The travel time as a function of depth is shown in Fig. 5 for the ray trace of Fig. 2.

The curve in Fig. 5 is effectively the wavefront as it passes the range of the receiver. The part of the curve up to 0.84 ms is the spherical wavefront representing the direct ray path from the source to the range of the receiver. The later sections of the curve correspond to the surface reflection of the wavefront. The reflection from the concave surface beneath the wave crest has caused the wavefront to fold over on itself. The sharp reversals of the wavefront occur at the caustics. The dashed curves extrapolate the wavefront into the caustic shadow.

Intersections of the wavefront with the line at the receiver depth (0.145 m) show the arrival times of the pulses which follow the ray paths of Fig. 3. In wavefront modeling, the arrival times of the pulses are used to construct the expected waveform, which is shown as the thicker line in Fig. 6. The thinner line waveform in Fig. 6 is the experimental result for run 104, ping 36.

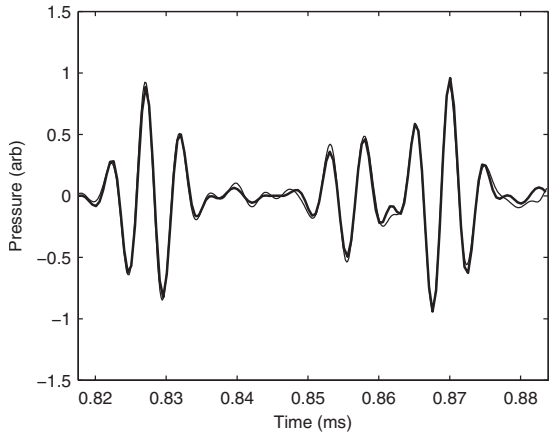

FIG. 6. Receiver waveforms for model (thick line) and data (thin line) for run 104, ping 36.

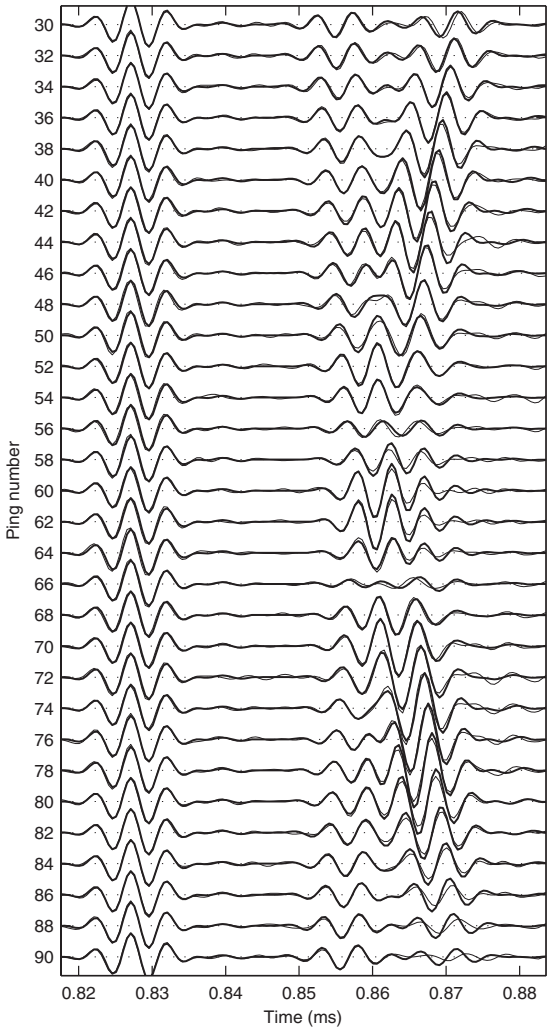

FIG. 7. Waveforms for run 104 and the ping numbers shown. The model is shown as thick lines and the data are shown as thin lines.

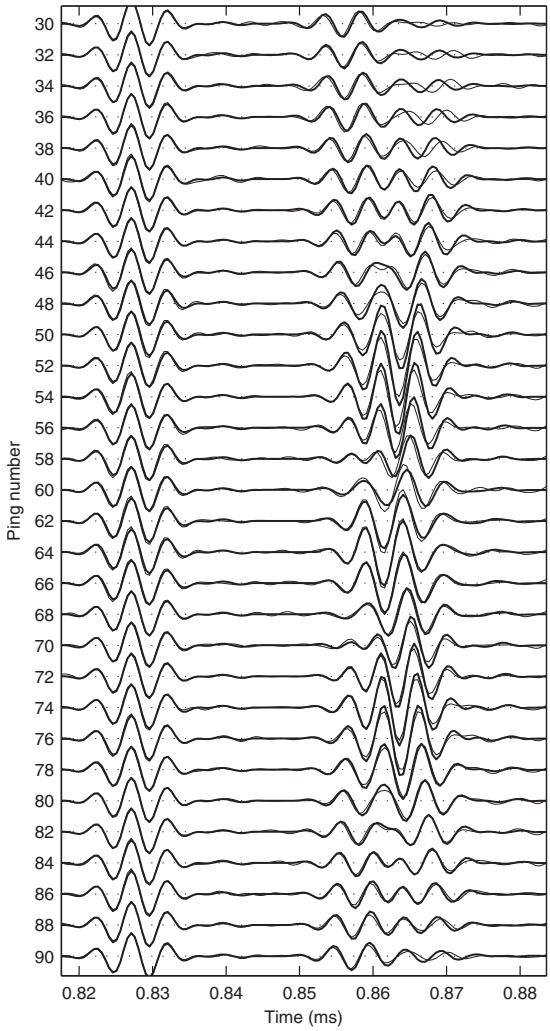

FIG. 8. Waveforms for run 103 and the ping numbers shown. The model is shown as thick lines and the data are shown as thin lines.

The first pulse in Fig. 6, centered at 0.828 ms, is the direct ray arrival. As described earlier, the model waveform for the direct arrival was found by averaging 120 experimental direct pulse waveforms. The slight differences evident between model and experiment for the direct pulse are due to the residual reverberation in the tank.

The second arrival in Fig. 6, centered at 0.855 ms, is from the ray which is reflected near the trough in Fig. 3. The third arrival, centered at 0.869 ms, is the combined pulse due to the two rays reflected near the wave crest in Fig. 3. These two rays have nearby ray angles as shown in Fig. 4 and very similar arrival times as shown in Fig. 5. The two rays are close to the upper caustic and are treated as a pair in the wavefront model.[3] The model waveform for the second and third arrivals is found by placing scaled and phase-shifted copies of the source pulse at the arrival times determined numerically from Fig. 5. The phase shift is achieved by taking the Fourier transform of the pulse, phase shifting the complex signal, and transforming back.

The theoretical expressions used to calculate the waveforms in Fig. 6 and the results to be shown in Figs. 7–10 were derived in Refs. 2 and 3. The amplitude and phase of isolated ray arrivals are given in Eq. (21) of Ref. 3. Pairs of rays which pass near a caustic and arrive with a travel time difference less than a quarter of a period (at the center frequency) give a single pulse described by an Airy function. The phase and amplitude of such pairs are given by Eq. (23) of Ref. 3. The pulse arrivals due to the caustic shadow to be shown in Figs. 7–10 are also described by an Airy function and have phase and amplitude determined using Eq. (23) of Ref. 3. Near a focus there are either three arrivals or one arrival and a caustic shadow. If the travel time differences are less than a quarter period the phase and amplitude of the combined pulse are found using the Pearcey function formula in Eq. (58) of Ref. 2 modified to allow for range dependence as described in Ref. 3. The formulas are summarized in Ref. 12.

IV. RESULTS

As the surface wave progresses all the above diagrams change smoothly. The positions of the focus and caustics move upward. The angles of the eigenrays change. The fold in the wavefront shown in Fig. 5 moves upward and the arrival times of the rays change. The amplitudes of the arrivals also change because they are related to the slope of $z^*(\theta)$. The amplitude of isolated ray arrivals is proportional to

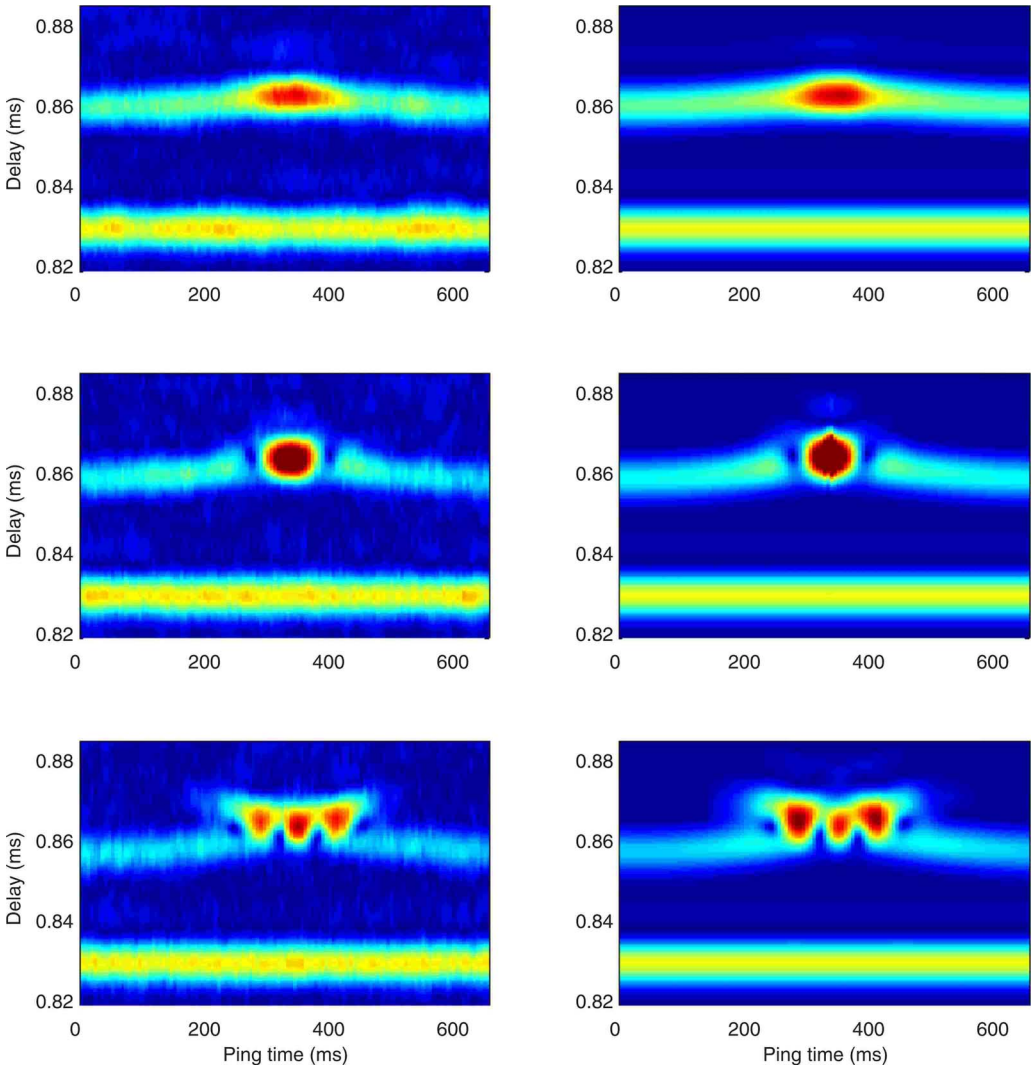

FIG. 9. (Color online) Signal amplitude contours. Individual pings are plotted vertically as a function of delay time. The horizontal axis is the transmission time of each ping. There are 120 pings in the 667 ms wave period. The left panels are the measured signals. The right panels show the wavefront model results. Top panels: run 101. Peak to trough wave height of 7 mm. Middle panels: run 102. Wave height of 16 mm. Bottom panel: run 103. Wave height of 24 mm.

$|dz^*/d\theta|^{-1/2}$ so steeper slope means smaller amplitude. In Fig. 4 the slope at −2° is smaller than the slope at −12° so, as expected, the direct arrival in Fig. 6 has greater amplitude than the isolated surface reflected arrival. Arrivals near a zero of $dz^*/d\theta$ occur in pairs and are treated as a pair using Airy functions to give a pulse of finite amplitude.[2,3]

The waveforms for a subset of pings for run 104 for a peak to trough wave height of 31 mm are shown in Fig. 7. The waveform of Fig. 6 is repeated four lines down in Fig. 7. For all pings in Fig. 7, the first pulse is the constant direct arrival, unaffected by the surface waves.

Waveforms for pings 30–34 show two surface reflected arrivals. The first surface arrival has a ray path similar to the isolated surface reflection in Fig. 3. The second surface arrival has no ray path and is due to the caustic shadow. If Figs. 2–5 were shown for pings 30–34, the upper caustic in Fig. 2 would be below the source depth. Correspondingly, the extremum of the ray depth curve in Fig. 4 would not intersect the receiver depth. The folded wavefront of Fig. 5 due to the surface reflection would intersect the receiver depth only once. However, the dashed extrapolation of the wavefront leads to a field in the shadow zone of the caustic and so pings 30–34 show a third arrival due to the caustic shadow.

Ping 36 has been discussed above. It has three surface reflections with the second and third arrivals very close together. Pings 36–82 all have three distinct surface reflections. The ray angles and arrival times of the individual eigenrays change smoothly as the surface wave moves. In pings 36–42 the second and third eigenrays arrive with a path difference less than a quarter wavelength which is equivalent to a travel time difference of less than a quarter of a period. As noted above the two surface reflections arriving close together are treated as a pair and the resulting field is given by an Airy function.[2,3]

Pings 44–74 all have three surface reflected eigenrays which interfere to produce maxima at pings 52 and 62 and minima at pings 56 and 66. The details of the interference is well reproduced by the wavefront model. For pings 76–82 the second and third surface reflections arrive close together and are treated as a pair as described above. Pings 84–90

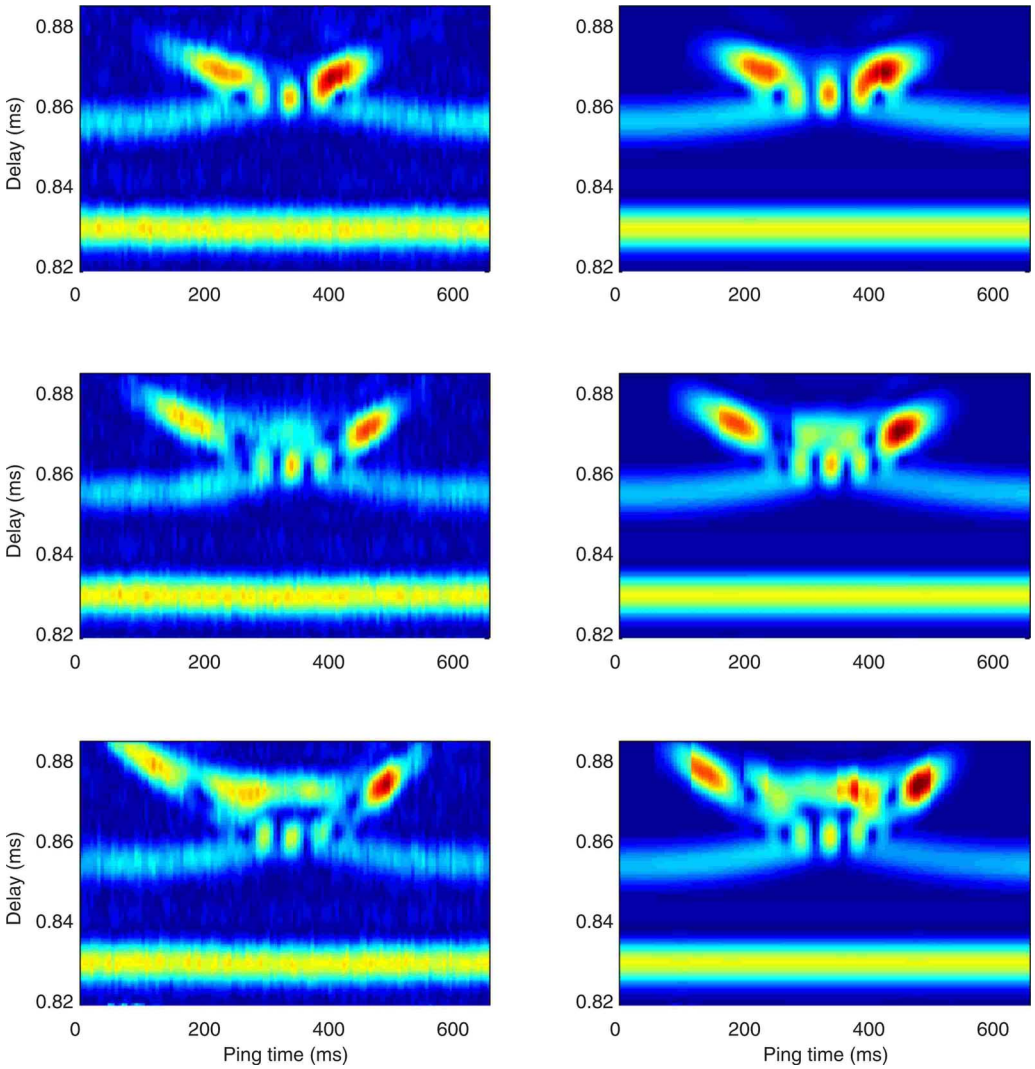

FIG. 10. (Color online) As for Fig. 9. Top panels: run 104. Peak to trough wave height of 32 mm. Middle panels: run 105. Wave height of 39 mm. Bottom panel: run 106. Wave height of 46 mm.

have only one eigenray but the second pulse observed in the waveforms is due to the shadow of the lower caustic in Figs. 4 and 5.

Figure 8 shows results for run 103. The wave height was 24 mm peak to trough. This wave height is smaller than for run 104 so the time spread of the surface reflections is less and no separated surface reflected pulses are observed. Nevertheless the same processes occur, as shown in Fig. 7. Pings 30–44 and 82–90 have one eigenray and a caustic shadow. Pings 46–54 and 72–80 have three eigenrays with the second and third arrivals treated as a pair. Pings 56–70 have three separate arrivals which interfere to give minima at pings 60 and 68 and a maximum at ping 64. The waveform for the surface reflected signal for ping 64 is almost exactly an inverted copy of the source signal and shows that the three surface reflected rays arrive almost simultaneously and reinforce each other.

The full set of data and model results is shown in Figs. 9 and 10. The waves in the tank experiment have a wavelength of 0.693 m and the peak to trough wave heights vary from 7 mm for run 101 up to 46 mm for run 106. To provide an oceanic context, when scaled by a factor of 225, the results correspond to transmission of 890 Hz pulses a distance of 275 m under ocean swells of period 10 s with peak to trough heights from 1.6 m (run 101) to 10.4 m (run 106).

Each panel in Figs. 9 and 10 shows contours of signal amplitude made by plotting the absolute value of the Hilbert transform of the waveform. Each ping is plotted vertically as a function of time, and the time scale is the same as in Figs. 7 and 8. The horizontal axis is the start time of each ping. There are 120 pings in each panel covering the 667 ms period of the surface waves. In all cases the central pings coincide approximately with the wave crest and the first and last pings occur at the wave trough. The waveforms in Fig. 8 are a subset of the data in Fig. 9, bottom panels. The waveforms in Fig. 7 are a subset of the data in Fig. 10, top panels.

The top panels in Fig. 9 show data and model for run 101 with a peak to trough wave height of 7 mm. The corresponding ray diagram would show weak focusing to a focus beyond the range of the receiver with no caustic present. The surface reflected signal is slightly delayed compared to the first and last pings because of the extra distance to the surface. The signal is increased in amplitude due to the converging effect of reflection from the curved surface.

The middle panels in Fig. 9 show data for run 102 with a peak to trough wave height of 16 mm. The corresponding ray diagram would show that the focus is formed just before the range of the receiver and the two caustics are very close together. This gives very strong enhancement of the received signal and a rapid and intense focus as the wave passes. It is this sort of strong signal enhancement that is a major complication for underwater acoustics communications systems.

The bottom panels in Fig. 9 show data for run 103 with a peak to trough wave height of 24 mm. A subset of the waveforms for this figure has been shown in Fig. 8. There is strong reinforcement in the center of the pattern when the surface wave is midway between source and receiver and the three surface reflected rays similar to those of Fig. 3 arrive almost simultaneously as noted above.

The strong signals at ping times of 280 and 420 ms in the bottom panel of Fig. 9 come from near the caustic. Two rays arrive very close together and give strong maxima near the caustics. At times before 280 ms and after 420 ms the surface reflected signal is due to the sound in the shadow zone of the caustics and the sound energy decays steadily with distance from the caustic.

The top panel in Fig. 10 is for run 104 and a wave height of 31 mm. Some of the waveforms have been shown in Fig. 7. At the center of the pattern two of the surface reflected rays arrive simultaneously and they reinforce to give the local maximum in Fig. 10 and pings 60–62 of Fig. 7. The third arrival from the crest of the wave is sufficiently delayed compared to that for run 103 that it does not reinforce the other two rays and there is smaller overall amplitude than for run 103.

The middle and lower panels in Fig. 10 are for runs 105 and 106 with wave heights of 39 and 46 mm, respectively. There are single arrivals for the earlier and later pings in each panel. In the center of each pattern two of the surface reflected rays arrive simultaneously and reinforce. The third surface arrival comes later and is somewhat separated from the other two. For the pings near but not at the center there are three distinct surface arrivals corresponding to the three arrivals of Fig. 5. As the wave progresses the surface reflected pulses partly overlap and give rise to the complicated interference patterns seen in both data and model results.

V. DISCUSSION AND CONCLUSIONS

The experimental results show that the presence of surface waves significantly alters propagation conditions for transmission and reception of underwater acoustics signals. It is clear that communications systems need to be designed to allow for rapid changes in signal level and rapid changes in interference from multiple paths.

The good agreement between theory and experiment shown in Figs. 6–10 is confirmation that the wavefront modeling method gives an accurate description of the propagation. The model is based on a ray interpretation of the propagation and correctly predicts the amplitude, phase, and travel time of pulses along each ray path.

Agreement between theory and experiment is not perfect. There is some noise in the data, as can be seen from the left panels of Figs. 9 and 10. The main source of difference between theory and experiment is probably noise in the measurement of the surface wave height. The focusing effect of a concave reflector is very sensitive to the details of the surface. This is because the ray trace uses both height and slope of the water surface and relies on smooth variation as the launch angle changes. It was necessary to smooth the surface waves by sampling every 3 cm in range and fitting a smooth curve to the surface wave data points.

Even though the experiment was conducted at a nominal frequency of 200 kHz and a wavelength of 7.5 mm, scaling the waves to a nominal swell period of 10 s shows that it is actually a low frequency situation. The good agreement of the wavefront modeling ray based approach is surprising given that the wave heights of up to 46 mm lead to path differences of only one or two wavelengths.

The experiment has shown the variations in signal travel time, amplitude, and phase associated with reflections from surface waves. The close agreement between theory and experiment shows that the interpretation in terms of pulse propagation along ray paths is physically correct.

ACKNOWLEDGMENT

The support of the Office of Naval Research, Grant No. N00014-04-1-0728, is gratefully acknowledged.

[1]J. C. Preisig and G. B. Deane, "Surface wave focusing and acoustic communications in the surf zone," J. Acoust. Soc. Am. **146**, 2067–2080 (2004).
[2]C. T. Tindle, "Wavefronts and waveforms in deep-water sound propagation," J. Acoust. Soc. Am. **142**, 464–475 (2002).
[3]C. T. Tindle and G. B. Deane, "Shallow water sound propagation with surface waves," J. Acoust. Soc. Am. **117**, 2783–2794 (2005).
[4]F. B. Jensen, W. A. Kuperman, M. B. Porter, and H. Schmidt, *Computational Ocean Acoustics* (Springer-Verlag, New York, 1993).
[5]M. G. Brown, "The transient wave fields in the vicinity of cuspoid caustics," J. Acoust. Soc. Am. **79**, 1367–1384 (1986).
[6]J. A. Ogilvy, "Wave scattering from rough surfaces," Rep. Prog. Phys., **50**, 1553–1608 (1987).
[7]J. A. Ogilvy and H. M. Merklinger, *Theory of Wave Scattering From Random Rough Surfaces* (Hilger, New York, 1991).
[8]C. K. Frederickson and P. L. Marston, "Transverse cusp diffraction catastrophes produced by the reflection of ultrasonic tone bursts from a curved surface in water: Observations," J. Acoust. Soc. Am. **92**, 2869–2876 (1992).
[9]C. K. Frederickson and P. L. Marston, "Travel time surface of a transverse cusp caustic produced by reflection of acoustical transients from a curved metal surface in water," J. Acoust. Soc. Am. **95**, 650–660 (1994).
[10]K. L. Williams, J. S. Stroud, and P. L. Marston, "High-frequency forward scattering from Gaussian spectrum, pressure release, corrugated surfaces. I. Catastrophe theory modeling," J. Acoust. Soc. Am. **96**, 1687–1702 (1994).
[11]See EPAPS Document No. E-JASMAN-125-041901 for movies of experimental waveforms and modeling results. For more information on EPAPS, see http://www.aip.org/pubservs/epaps.html.
[12]C. T. Tindle, G. Deane, and J. Preisig, "Multipath reflection from surface waves," Acoustics 08 Paris Proceedings, Societe Francaise d'Acoustique.